JOURNAL OF GEOPHYSICAL RESEARCH, VOL. 96, NO. C6, PAGES 10,581–10,592, JUNE 15, 1991

A Bio-optical Model of Antarctic Sea Ice

KEVIN R. ARRIGO

Department of Biological Sciences, University of Southern California, Los Angeles

CORNELIUS W. SULLIVAN[1]

Graduate Program in Ocean Sciences, Hancock Institute of Marine Studies, University of Southern California, Los Angeles

JAMES N. KREMER

Department of Biological Sciences, University of Southern California, Los Angeles

Biogenic particulate material in sea ice can substantially influence the spectral irradiance within the ice sheet and underlying seawater. In order to simulate accurately seasonal changes in light conditions in situ, the biomass changes of the sea ice microbial community must be considered. Here we attempt to provide an improved description of the optical regime within sea ice by combining information provided by models of radiative transfer in sea ice and snow and models of solar spectral irradiance with formulations describing the attenuation of spectral irradiance by particulates observed in sea ice in McMurdo Sound, Antarctica. Emphasis has been placed on the role of biogenic particles in visible light attenuation with the intent of developing a bio-optical model that more rigorously describes their influence on radiative transfer processes as they occur in nature. Model results simulating seasonal changes in both photosynthetically active radiation and its spectral distribution agree well with measured under-ice spectral irradiance. Results reveal how changes in microalgal concentrations, as well as their photophysiological characteristics influence both the quantity and quality of downwelled light in sea ice and in the upper layers of the ice-covered oceans.

Introduction

Radiative transfer models describing the wavelength-dependent optical properties of Arctic snow and congelation ice have greatly aided the study of heat and mass balance in the polar regions as well as furthered our understanding of light distribution through the ice sheet [*Perovich and Grenfell*, 1982; *Grenfell*, 1983; *Grenfell and Perovich*, 1986]. *Maykut and Grenfell* [1975] also recognized the potential importance of these models to the understanding of primary productivity in ice-covered oceans. The usefulness of most radiative transfer models is limited, however, by their assumption of structural homogeneity and exclusion of particulate absorption. Here we combine information provided by existing radiative transfer models with a detailed treatment of the effects of biogenic particles on visible light attenuation in sea ice. The goal is to develop a bio-optical model which can account for seasonal changes in the physical, chemical, and biological processes influencing radiative transfer in sea ice.

The General Case

The magnitude of downwelling spectral irradiance at a given depth within a structurally homogeneous medium depends upon surface reflection of direct and diffuse incident irradiance as well as attenuation within the medium:

$$E_d(z,\lambda) = E_d(0,\lambda)\, e^{(-K_d(\lambda)z)} \quad (1a)$$

and

$$E_d(0,\lambda) = (1-R_{sun}(0,\lambda))E_{dsun}(0,\lambda) + (1-R_{sky}(0,\lambda))E_{dsky}(0,\lambda) \quad (1b)$$

where $E_d(z,\lambda)$ is the spectral irradiance (μEin m^{-2} s^{-1} nm^{-1}) at depth z (m) and wavelength λ (nm), $E_d(0,\lambda)$ is the spectral irradiance at the sea ice surface, $R(0,\lambda)$ is the specular reflection at the sea ice surface (0-1) with the subscripts sky and sun denoting the diffuse and direct components, and $K_d(\lambda)$ is the bulk diffuse spectral attenuation coefficient (m^{-1}). Because sea ice undergoes dramatic temporal and spatial changes in its physical [*Cox and Weeks*, 1975, 1986] and biological [*Bunt and Lee*, 1970; *Palmisano and Sullivan*, 1983] characteristics, there is no single value of $K_d(\lambda)$ that adequately describes the optical properties of sea ice and snow under all conditions. Rather, this coefficient changes with both physical and biological processes that occur within the snow and ice cover [*Maykut and Grenfell*, 1975]. The diffuse attenuation coefficient for sea ice is dependent upon absorption and scattering properties which vary with bubble density, brine volume, and particle type and concentration. To account for these variations, more detailed formulations for $K_d(\lambda)$ within the ice sheet have been adopted in the present model. Only a brief description of these processes will be provided here; specific formulations can be found in Table 1.

The Model

Formulations relating radiative transfer in particle-free sea ice and snow to their physical structure are derived from existing theoretical radiative transfer models [*Perovich and Grenfell*, 1982; *Grenfell*, 1983; *Grenfell and Perovich*, 1986] and from spectral irradiance data collected in both Arctic and Antarctic regions. It is assumed that data collected from the

[1]Also at Department of Biological Sciences, University of Southern California, Los Angeles.

Paper number 91JC00455.
0148-0227/91/91JC-00455$05.00

TABLE 1. Coefficients Used in the Bio-optical Model to Define the Optical Parameters for the Ice Sheet

Variable	Comment	Regression Equation	R^2	Data Source
$K_{ds}(\lambda)$	dry snow	$104 - 0.38\lambda + 4.248 \times 10^{-4} \lambda^2$	0.96	*Grenfell and Maykut* [1977]
	wet snow	$72.36 - 0.27\lambda + 2.883 \times 10^{-4} \lambda^2$	0.98	*Grenfell and Maykut* [1977]
$R_{sun}(0,\lambda)$	$\theta \leq 1.4$	$(1.8736 \times 10^{-2})\ 10^{0.153160}$	0.99	*Kirk* [1983]
	> 1.4	$(3.6779 \times 10^{-4})\ 10^{0.15050}$	0.96	*Kirk* [1983]
$K_{df}(\lambda)$	fresh ice	$0.092 - 3.522\lambda \times 10^{-4} + 3.632 \times 10^{-7} \lambda^2$	0.97	*Grenfell and Perovich* [1981]
$K_{di}(z,\lambda)$	eutectic (<-21°C)	$65.114 - 0.23551\lambda + 2.3078 \times 10^{-4} \lambda^2$	0.97	*Perovich* [1979]
$K_{di}(z,\lambda)$	vs brine volume	$K_{df}(\lambda) + Vbb$	0.94	*Grenfell* [1983]
b	superscript in Vbb	$4.31 - 0.0213\lambda + 3.66 \times 10^{-5} \lambda^2 + 1.98 \times 10^{-8} \lambda 3$	0.92	*Grenfell* [1983]
$K_{dip}(\lambda)$	platelet ice	$3.5233 - 1.83 \times 10^{-2} \lambda + 3.29 \times 10^{-5} \lambda^2 - 1.81 \times 10^{-8} \lambda^3$	0.93	this study

Equations were obtained from least-squares regression of data from sources shown. $K_{ds}(\lambda)$, $K_{df}(z,\lambda)$, $K_{di}(\lambda)$, and $K_{dip}(\lambda)$ are the diffuse spectral attenuation coefficient for dry snow, freshwater ice, congelation ice, and platelet ice, respectively (m^{-1}), $R_{sun}(0,\lambda)$ is the specular reflection at the sea ice surface (unitless), θ is the solar zenith angle (radians).

Arctic is directly applicable to the Antarctic. Strictly speaking, this is probably not the case, especially for pack ice which is generally thinner [*Thorndike et al.*, 1975] and less saline [*Wadhams*, 1986] in the Antarctic than in the Arctic. However, fast ice sampled in McMurdo sound was found to be structurally similar to Arctic fast ice, including its tendency to horizontal C axis orientation, although it was also slightly less saline [*Wadhams*, 1986]. Fortunately, differences in sea ice salinity and ice thickness between fast ice types in the two regions are minor and have been accounted for in the present model.

Atmospheric Spectral Irradiance, $E_d(\lambda)$

By coupling equations estimating solar declination [*Spencer*, 1971] and solar elevation [*Kirk*, 1983] to a simplified spectral atmospheric irradiance model [*Brine and Iqbal*, 1983], a time-and-latitude-dependent algorithm has been developed which predicts both the direct and diffuse components of spectral irradiance within the visible range (400-700 nm). To obtain spectral irradiance at the sea ice surface, the resulting prediction of spectral irradiance is adjusted to account for cloud cover [*Reifsnyder and Lull*, 1965].

Specular Reflection, $R(0,\lambda)$

Reflection occurs at the interface of two media with different refractive indices. The refractive index for air, ice, and water are 1.00, 1.31, and 1.33, respectively. Because the refractive indices of ice and water are so similar, $R(0,\lambda)$ is negligible at the interface of these two media. This is not true for air/ice, however, and under diffuse sky conditions the value for $R_{sky}(0,\lambda)$ is 0.05 [*Perovich and Grenfell*, 1982], with no spectral dependence within the visible. In the model $R_{sun}(0,\lambda)$ is assumed to be a function of solar zenith angle in a manner analogous to that observed for a flat ocean surface [*Preisendorfer*, 1976], varying from 0.02 to 1.00.

Spectral Diffuse Attenuation of Snow, $K_{ds}(\lambda)$

Light attenuation by snow is a function of absorption and volume scattering; the former determines wavelength dependence and the latter dominates the magnitude of attenuation. Due to the highly scattering nature of individual snow grains, the spectral attenuation coefficient of snow (15 to 20 m^{-1} at 470 nm) is often an order of magnitude higher than that of ice (1.5 to 2.0 m^{-1} at 470 nm) [*Grenfell and Maykut*, 1977]. Observations indicate that $K_{ds}(\lambda)$ is proportional to snow grain size, which varies with age [*Stephenson*, 1967], and inversely proportional to snow density and water content [*Perovich et al.*, 1986]. The bio-optical model makes no attempt to account for snow grain metamorphism and assumes that the snow pack is composed of large, densely packed grains. Changes in the liquid water content of the snow pack will be accounted for, however, since $K_{ds}(\lambda)$ for wet snow is about half that observed for dry snow [*Grenfell and Maykut*, 1977].

Spectral Diffuse Attenuation of Congelation Ice, $K_d(z,\lambda)$

The diffuse attenuation coefficient of sea ice, $K_d(\lambda)$, varies with depth and is related to ice type (congelation or platelet), brine volume (a function of temperature and sea ice salinity), bubble density, as well as particle concentration and type (described below). In the model, bubble density is assumed to remain constant (0.86 g cm^{-3}), and the diffuse attenuation coefficient for particle-free sea ice, $K_{di}(z,\lambda)$, varies only as a function of brine volume. We used the relationships between $K_{di}(z,\lambda)$ and sea ice temperature and growth rate given by *Grenfell* [1983] to approximate the relationship between $K_{di}(z,\lambda)$ and brine volume (Figure 1). This was achieved by converting ice growth and temperature data to brine volumes using equations given by *Cox and Weeks* [1983, 1986]. Because of the small data set and lack of resolution at low brine volumes, it is difficult to determine the precise relationship between $K_{di}(\lambda)$ and brine volume in this way. However, based upon low values for $K_{di}(\lambda)$ determined for bubble and brine-free polycrystalline ice [*Grenfell and Perovich*, 1981] and higher but relatively constant values determined for bubble-free sea ice with brine volumes greater than 40 ppt [*Grenfell*, 1983] there appears to be a rapid, nonlinear increase in $K_{di}(\lambda)$ in response to rising brine volume. Consequently, the relationship given in Table 1 and illustrated in Figure 1 was chosen. This is somewhat inconsistent with other results from *Grenfell* [1983] which indicate that $K_{di}(\lambda)$ declines slightly as the sea ice warms (and brine volume increases). However, the calculated brine volumes were all quite high (40-110 ppt) for these cases, and changes in $K_{di}(\lambda)$ were relatively small.

Special consideration must be given to eutectic ice. As the temperature of sea ice drops below the eutectic point (-21°C) and solid salts form, $K_{di}(z,\lambda)$ at 470 nm increases dramatically from less than 1 m^{-1} to about 5 m^{-1}. The change at 700 nm is even more pronounced, increasing from 2 m^{-1} to more than 13 m^{-1} below the eutectic point [*Perovich*, 1990]. Because the increase in $K_{di}(z,\lambda)$ is more than enough to mask changes in any other sea ice parameter, as the ice drops below the eutectic

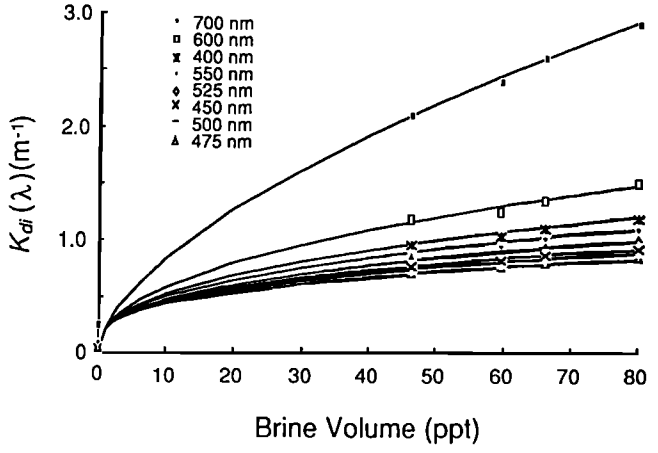

Fig. 1. The relationship between brine volume (parts per thousand) and diffuse attenuation, $K_{di}(\lambda)$ for pure sea ice used in the bio-optical model. Data points for brine volumes greater than 40 ppt are derived from *Grenfell* [1983]. Brine volumes were determined using sea ice salinity, growth rate, and temperature provided by *Grenfell* [1983] for each model run with equations relating these variables to brine volume from *Cox and Weeks* [1983]. Data points for brine volume = 0 ppt are from *Grenfell and Perovich* [1981].

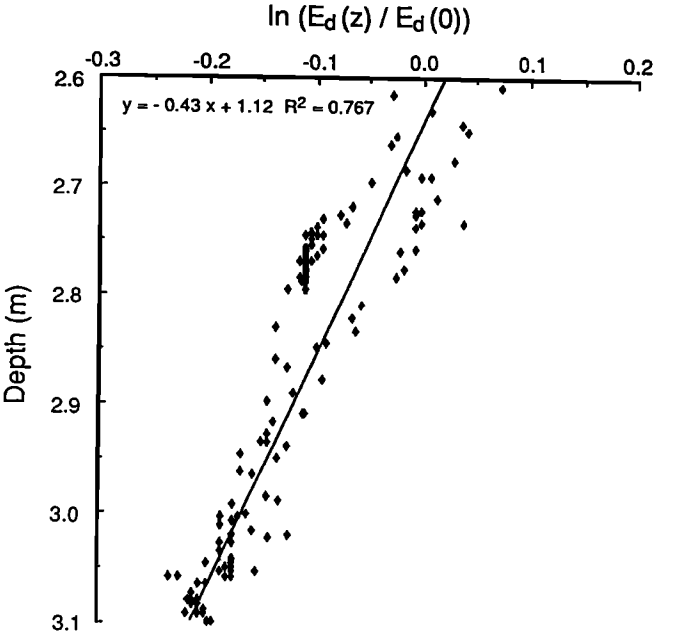

Fig. 2. Plot of ln $[E_d(z)/E_d(0)]$ versus depth in the platelet ice. $E_d(z)$ is the downwelling irradiance at depth z and $E_d(0)$ is the downwelling irradiance at the shallowest depth where measurements were obtained. The negative slope of the regression (-0.43) provides an estimate of the average attenuation coefficient, $K_{dip}(z)$. Data collected from McMurdo Sound, Antarctica, on November 21, 1989.

point, other changes in sea ice brought about by low temperature will be ignored.

The Spectral Diffuse Attenuation of Platelet Ice, $K_{dip}(z,\lambda)$

Platelet ice is a layer of loosely consolidated disk-shaped crystals, roughly 1 mm thick and 10 cm in diameter, commonly found beneath congelation ice in McMurdo Sound and in other ice-covered regions near ice shelves [*Lewis and Weeks*, 1970]. Due to their spacing and random orientation, there is a large amount of seawater (80% of total layer volume) between ice platelets [*Bunt and Lee*, 1970]. Since a large proportion of the biological community resides in this layer, either attached directly to the ice platelets or suspended in the interstitial seawater (*K. Arrigo*, unpublished data, 1989), the optical properties of this layer must be considered.

The diffuse attenuation coefficient, $K_{dip}(z)$, as well as the spectral diffuse attenuation coefficient, $K_{dip}(z,\lambda)$, were estimated for a 0.7-m platelet layer in McMurdo Sound on November 21, 1989. A Biospherical Instruments MER 1010 spectroradiometer was positioned beneath the platelet ice where both $E_d(z,\lambda)$ and $E_d(z)$ (irradiance integrated from 400 to 700 nm, referred to as photosynthetically active radiation, or PAR), were recorded as the instrument was raised vertically through the lower 0.5 m. The upper 0.2 m layer of platelet ice was excluded from this analysis due to the high chlorophyll *a* (chl *a*) concentration found there, while the lower 0.5 m appeared to be free of significant particulate contamination (<1 μg chl *a* L^{-1}). By regressing ln $[E_d(z)/E_d(0)]$ against depth (where $E_d(0)$ is the downwelling irradiance at the shallowest depth where measurements were obtained), $K_{dip}(z)$ was estimated to be 0.4 m^{-1} (Figure 2). This is approximately one third the value of 1.5 m^{-1} typically obtained for congelation ice in the same area. Due to low spectral sensitivity of the spectroradiometer, a similar regression approach could not be used with the spectral data. Instead, values for $K_{dip}(z,\lambda)$ were estimated from spectral irradiance measured at the extreme upper and lower boundaries of the particle-free platelet ice using the equation

$$K_{dip}(z,\lambda) = \frac{1}{\Delta z} \ln \frac{E_d(z,\lambda)}{E_d(z+\Delta z,\lambda)}$$

where $E_d(z,\lambda)$ and $E_d(z+\Delta z,\lambda)$ are the downwelling spectral irradiances at depths z and $z+\Delta z$, respectively, and Δz is the depth increment between measurements (0.5 m). Estimated values for $K_{dip}(z,\lambda)$ are shown in Figure 3 with the solid curve representing the best fit of the data as determined by third order least squares polynomial regression. The resulting regression equation (see Table 1) was used to define the spectral variability of $K_{dip}(z,\lambda)$ in the bio-optical model.

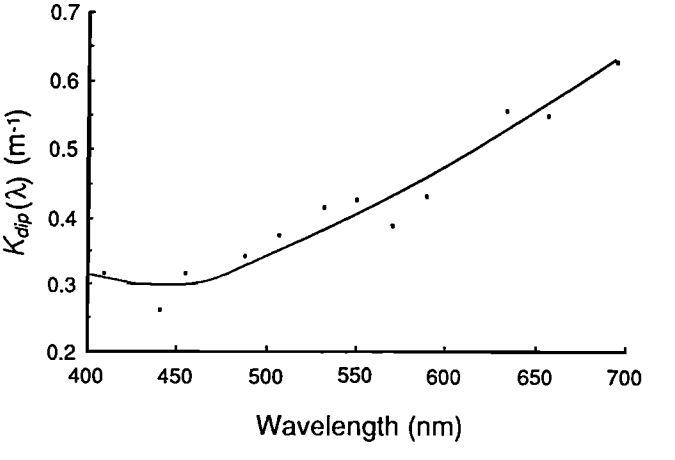

Fig. 3. Diffuse attenuation coefficient spectrum for platelet ice, $K_{dip}(z,\lambda)$. The solid curve represents the best fit of the data as determined by third order least squares polynomial regression. Data collected from McMurdo Sound, Antarctica, on November 21, 1989.

Particulate Attenuation: Description

In the austral spring, the land fast sea ice in McMurdo Sound harbors a growing microbial community dominated by diatoms but also including other microalgal species, bacteria, and protists [*Palmisano and Sullivan*, 1983; *Sullivan and Palmisano*, 1984; *Sullivan et al.*, 1985]. The community is generally restricted to the bottom 0.2 m of congelation ice and the platelet layer below [*Palmisano and Sullivan*, 1983] where microalgae may reach chl *a* concentrations of 2-5 mg L^{-1} late in the season (December). Field observations in McMurdo Sound indicate that during the period October through December, the microbial community can have a significant influence on the amount and spectral distribution of PAR transmitted through sea ice [*Palmisano et al.*, 1987; *SooHoo et al.*, 1987]. Attenuation of downwelled irradiance is not uniform within this spectral range because sea ice microalgae, with chl *a* as their major light absorbing pigment, have two absorption peaks in vivo, one broad peak centered at 440 nm and another narrower peak at 680 nm, with little absorption in the green-yellow region (575-650 nm) (Figure 4). In addition, accessory pigments such as fucoxanthin absorb maximally around 450-550 nm.

Microalgae in the upper portion of the ice sheet absorb PAR that would otherwise be transmitted deeper into the ice, and due to their differential spectral absorption, also alter its spectral distribution. To maximize photosynthetic efficiency (α, the amount of carbon fixed per unit incident irradiance), algae at lower depths within the sea ice photoadapt to PAR of decreased magnitude and altered spectral form by modifying their light harvesting characteristics. Consistent with this idea, *SooHoo et al.* [1987] reported distinct absorption spectra and specific absorption coefficients, $a^*(\lambda)$ for congelation and platelet ice microalgal communities, the latter exhibiting enhanced absorption in the 450-550 nm range. This enhanced absorption by platelet ice algae is a necessary adaptation to offset the diminished amount of PAR available from above [*SooHoo et al.*, 1987].

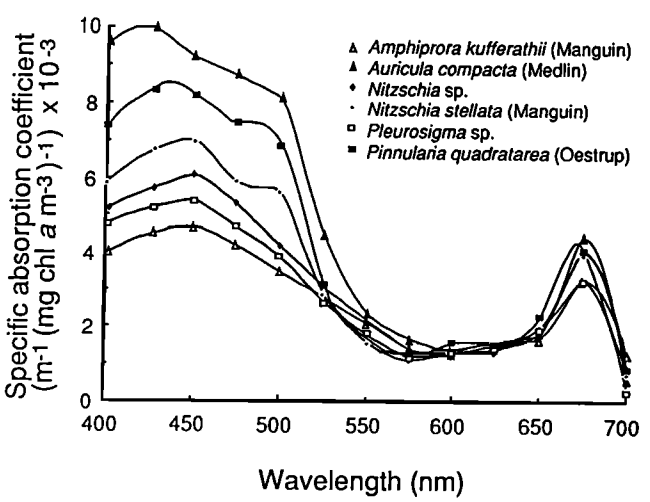

Fig. 4. Chlorophyll *a* specific absorption coefficients for the most abundant sea ice microalgal species in McMurdo Sound, Antarctica. Spectra were determined from individual cells using the equation of *Morel and Bricaud* [1981], $a^*(\lambda)=a_{sol}^*(\lambda)\,(3Q_a(\lambda))/(2\rho'(\lambda))$. Single-cell Q_a (absorption efficiency) spectra were determined microphotometrically (for details of this method see *Iturriaga et al.* [1988]), and used to estimate ρ' using equation 1 from *Morel and Bricaud* [1981]. The coefficient $a_{sol}^*(\lambda)$ was estimated using the pigment specific absorption coefficients reported in *Bidigare et al.* [1989].

Particulate Attenuation: Formulations

The spectral diffuse attenuation coefficient for sea ice has been partitioned into components for pure sea ice and associated particles so that at a given depth, $K_d(z,\lambda)$ is approximated as

$$K_d(z,\lambda) = K_{di}(z,\lambda) + K_{dp}(z,\lambda) \quad (2)$$

where $K_{di}(z,\lambda)$ and $K_{dp}(z,\lambda)$ are spectral diffuse attenuation coefficients (m^{-1}) for particle-free ice and associated particles, respectively. This formulation is similar to one used by *Smith and Baker* [1978] to describe the bulk optical properties of seawater. The model estimates $K_d(z,\lambda)$ independently for each 0.01-m layer within the sea ice based upon depth-dependent changes in $K_{di}(z,\lambda)$ and $K_{dp}(z,\lambda)$.

With the exception of the extreme upper ice surface, the angular distribution of irradiance is constant throughout the ice sheet (asymptotic distribution). For this reason, and because backscattering by particles has been ignored, the diffuse downwelling spectral attenuation coefficient due to particles (which is equivalent to the attenuation coefficient for scalar irradiance in an asymptotic field) at any depth z can be approximated by

$$K_{dp}(z,\lambda) = \frac{a_m(z,\lambda) + a_d(z,\lambda)}{\bar{\mu}} \quad (3)$$

[*Kirk*, 1983; *Sathyendranath et al.*, 1989] where $a_m(z,\lambda)$ and $a_d(z,\lambda)$ are the particulate absorption coefficients (m^{-1}) for microalgae and detritus, respectively, and $\bar{\mu} = 0.656$ [*Grenfell*, 1983] is the mean cosine of the angular distribution of irradiance. To account for changes in the particulate absorption coefficient due to shifts in microalgal concentrations, $a_m(z,\lambda)$ for sea ice microalgae can be computed as

$$a_m(z,\lambda) = a^*(z,\lambda)\,C(z) \quad (4)$$

where $a^*(z,\lambda)$ is the chl *a* specific absorption coefficient for sea ice microalgae ($m^2\ mg^{-1}$) and $C(z)$ and is the chl *a* concentration ($mg\ m^{-3}$), both at depth z.

The coefficient $a^*(\lambda)$ observed for phytoplankton exhibits marked interspecific variability [*Sathyendranath et al.*, 1987] depending primarily upon the composition and concentration of intracellular pigments, as well as cell size [*Morel and Bricaud*, 1981]. Taxonomic differences in $a^*(\lambda)$ were also apparent for a variety of sea ice microalgal species collected from McMurdo Sound in 1988 (Figure 4). Although the absorption spectra shown in Figure 4 may be used individually in equation (4), it is possible to combine values of $a^*(z,\lambda)$ for different algal species to arrive at a bulk $a^*(z,\lambda)$ for the community. This is defined as

$$a^*(z,\lambda) = \sum_{i=1}^{n} \psi_i\, a_i^*(z,\lambda) \quad (5)$$

where $a_i^*(z,\lambda)$ is the specific absorption coefficient for species i, n is the number of species, and ψ_i is a weighting factor corresponding to the relative abundance (0-1) of species i in the community.

Specific absorption also varies for algal communities located at different vertical positions within sea ice [*SooHoo et al.*, 1987]. Figure 5 illustrates how estimates of $a^*(\lambda)$ (made using the method of *Kiefer and SooHoo* [1982]) for congelation

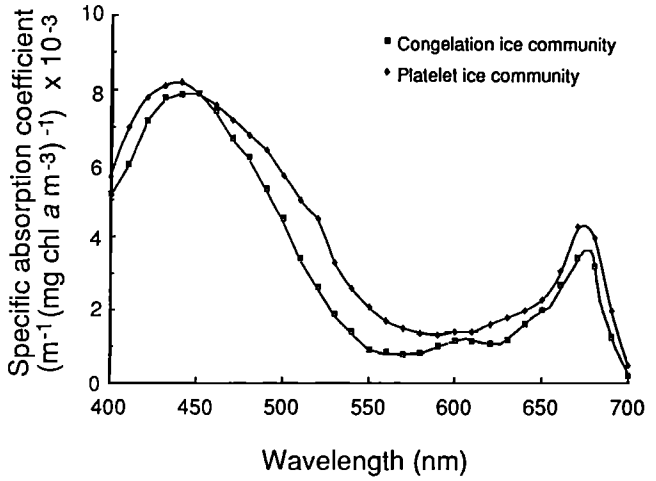

Fig. 5. Specific absorption coefficient spectra for congelation and platelet ice communities collected in McMurdo Sound, Antarctica (for method see *Kiefer and SooHoo* [1982]). These are used as default values for $a^*(\lambda)$ in the bio-optical model.

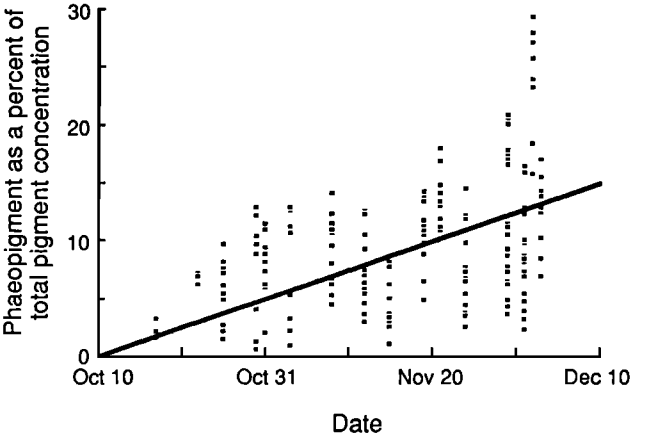

Fig. 6. Seasonal change in the relative phaeopigment abundance as measured fluorometrically in sea ice particulate matter from McMurdo Sound, Antarctica, between October 15 and December 5, 1989.

and platelet ice communities varied during the spring microalgal bloom in McMurdo Sound in 1989. These estimates can be used as default values in the bio-optical model if specific taxonomic data are not available.

No rigorous means currently exists to quantify either detrital concentration or its specific absorption in situ, so detrital absorption is modeled here as an arbitrary percentage of the microalgal absorption of PAR, which is chosen by the user. Because phaeopigments (phaeophorbide + phaeophytin) are degradation products of chl *a*, phaeopigment concentrations have been used by others as an index of detrital absorption [*Sathyendranath et al.*, 1989]. It may be possible then to infer appropriate values for the percent absorption by detrital particles from data on seasonal changes in chl *a* and phaeopigment concentrations (Figure 6). Equations (6) through (9) describe how the detrital absorption spectrum is calculated after defining its magnitude as a percent of total microalgal absorption between 400 and 700 nm. Note that this is not meant as a method of decomposing particulate absorption spectra into detrital and algal components, but rather a convenient way to define the desired magnitude of spectral absorption by detritus.

Absorption of total PAR by microalgae at depth z is computed as

$$a_m(z) = \int_{400}^{700} a_m(z,\lambda)\, d\lambda \qquad (6)$$

Because detrital absorption is to be modeled as a fraction of total microalgal absorption

$$a_d(z) = \delta\, a_m(z) \qquad (7)$$

where δ is the fraction of microalgal absorption equivalent to the desired magnitude of detrital absorption.

Equation 7 ensures that $a_d(z)$ is of the desired magnitude, but because the goal is to calculate its effect on downwelling spectral irradiance, it must be converted to $a_d(z,\lambda)$ with proper spectral form. Figure 7 shows absorption spectra for detritus obtained from sea ice in McMurdo Sound [*Iturriaga and Sullivan*, 1989]. Least squares regression indicates that the shape of this curve within the visible is adequately described by the equation

$$a_d(z,\lambda) = a_d(z,400)\, e^{-0.008(\lambda-400)} \qquad (8)$$

where $a_d(z,400)$ is the computed detrital absorption (m^{-1}) at λ=400, and λ is wavelength from 400 to 700 nm. Equation (8) defines the shape and magnitude of detrital absorption once $a_d(z,400)$ is calculated. Because detrital absorption is defined as a fraction of microalgal absorption, it is necessary to calculate the magnitude of $a_d(z,400)$ necessary to yield the required detrital absorption. This is done by integrating both sides of equation (8) from 400-700 nm and substituting in equation (7), obtaining

$$a_d(z,400) = \frac{\delta\, a_m(z)}{\int_{400}^{700} e^{-0.008(\lambda-400)}\, d\lambda} \qquad (9)$$

Once the relative contribution of detritus (δ) has been specified, the value of $a_d(z,400)$ given by equation (9) is substituted into equation (8) to obtain the spectral diffuse attenuation coefficient for detritus of the correct magnitude and spectral form.

Model Results and Discussion

K_d for Sea Ice With Low Particle Concentrations

A profile of PAR was measured within the interior (0.09-1.09 m) of a 2 m congelation ice sheet at noon on November

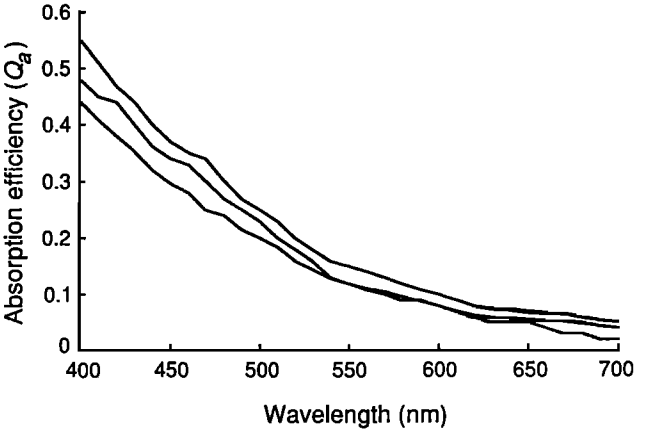

Fig. 7. Spectral absorption efficiency (Q_a) of individual detrital particles collected from McMurdo Sound sea ice as determined by microspectrophotometry [*Iturriaga and Sullivan*, 1991].

21, 1988 (Figure 8) in order to estimate the bulk diffuse attenuation coefficient (K_d) and compare it to values generated by the bio-optical model. Optical measurements were made by first drilling a vertical hole 1.3 m deep and 1.2 m in diameter into the congelation ice. A series of 2 cm diameter holes were then drilled horizontally into the sides of the main hole to a depth of 0.3 m, at 0.2-m intervals, starting 0.09 m from the surface. After covering the main hole with an opaque tarpaulin, a Biospherical Instruments QSL-100 PAR wand (with 4π collector) was inserted into each horizontal hole and scalar irradiance was measured. K_o was then computed according to the equation

$$K_o = \frac{1}{\Delta z} \ln \frac{E_o(z)}{E_o(z+\Delta z)}$$

where $E_o(z)$ and $E_o(z+\Delta z)$ are the scalar irradiances at depths z and $z+\Delta z$, respectively, and Δz is the depth increment between measurements. Assuming the irradiance field is asymptotic, K_o is equivalent to K_d used in the bio-optical model, allowing direct comparison with model results.

Predictions of K_d for the ice sheet were generated using as input the observed field conditions at the time the profile was made, assuming no particulates were present, and then averaging the resulting values for $K_d(z)$ over the depths of 0.09 to 1.09 m ($K_d(z)$ varies with depth depending upon sea ice temperature and salinity). Although chl *a* concentrations in the upper congelation ice at the time of sampling normally range from 0.01-1.0 μg L^{-1} (*K. Arrigo*, unpublished data, 1988), the bulk values of K_d determined from the PAR profile and predicted

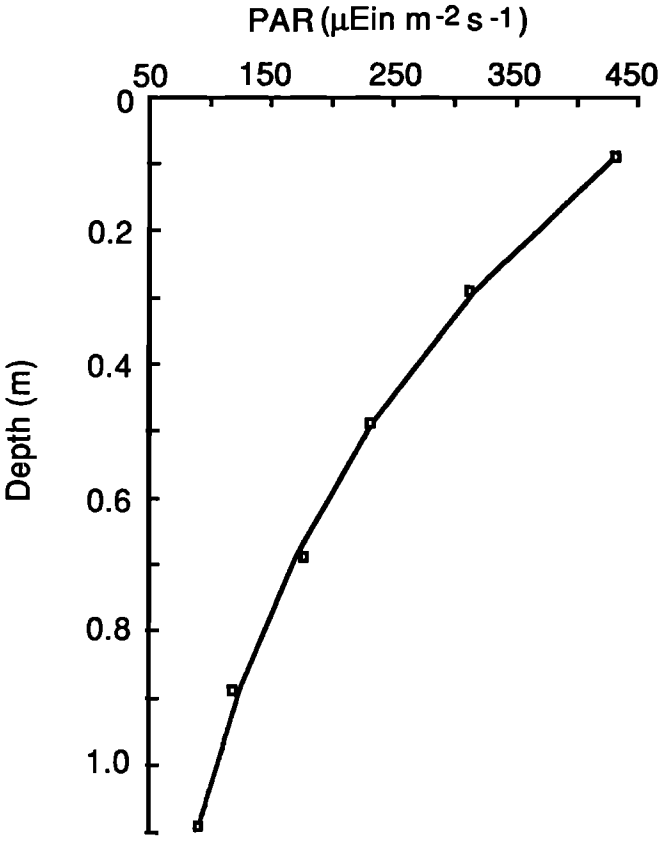

Fig. 8. Profile of PAR measured through the interior (0.09-1.09 m) of 2.25 m of congelation ice at noon on November 21, 1988. The open squares represent measured scalar irradiance and the solid curve represents the equation $E(z)=E_o(0.09)\exp(-Kz)$ where $E_o(0.09)$ is the scalar irradiance 0.09 m below the ice surface, and K = 1.55 m^{-1}.

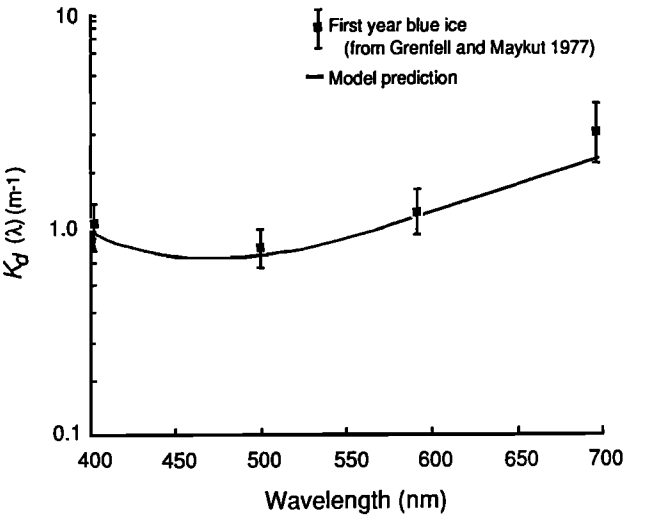

Fig. 9. Comparison of observed bulk spectral diffuse attenuation coefficient, $K_d(\lambda)$, with model predictions. Observations are from *Grenfell and Maykut* [1977] for interior first-year blue ice. Although model predictions are within the standard deviation of the measured $K_d(\lambda)$ at all wavelengths, substantial deviation from the mean occurs at 700 nm (note log scale of $K_d(\lambda)$). This may account for overestimates in spectral irradiance seen in the 600-700 nm range (see Figure 10).

by the bio-optical model (assuming no chl *a* was present) are in good agreement, yielding values of 1.55 m^{-1} and 1.46 m^{-1}, respectively. Moreover, model results show that a K_d of 1.55 m^{-1} can be achieved by assuming a mean chl *a* concentration of 0.3 μg L^{-1} throughout the sea ice interior, a concentration well within the range typically observed there.

Figure 9 illustrates how the predicted spectral shape of K_d compares with estimates obtained in the field by *Grenfell and Maykut* [1977] for interior white ice. Predictions were made assuming ice thickness = 1.5 m, surface temperature = -10°C, sea ice salinity = 5 ppt, and chl *a* = 0 (i.e. $K_d(\lambda)=K_{di}(\lambda)$). However, because field data were not available to fully define conditions for this model run, the comparison is only an approximation. Nevertheless, as seen in Figure 9, the spectral form of the predicted $K_d(\lambda)$ is within the range of expected measurement error, although a slight underestimate is apparent at longer wavelengths. This will be discussed later.

While the accuracy of the assumed relationship between $K_{di}(\lambda)$ and brine volume (Figure 1) cannot be determined directly, it can be tested indirectly by comparing model predictions of under-ice spectral irradiance at different sea ice temperatures, and thus different brine volumes, with spectral irradiance measured in the field under known conditions. Figure 10 illustrates how predictions of under-ice spectral irradiance change when the model is run varying only the surface temperatures between -5°C and -20°C. These results were compared to measured under-ice spectral irradiance in McMurdo Sound in late September 1984 when surface temperature was approximately -20°C and chl *a* concentrations were <0.5 μg L^{-1} (*C. Sullivan*, unpublished data, 1984). Clearly, agreement between predicted and observed spectral irradiance is superior when simulated surface temperature is near that measured in situ. This difference may be attributed to sea ice brine volume changes in response to varying sea ice temperature. For the -5°C case, assuming a sea ice salinity of 6 ppt (as determined by analyzing numerous ice cores), brine volume would be 60 and 150 ppt at the sea ice surface and bottom, respectively, averaging 91 ppt for the ice

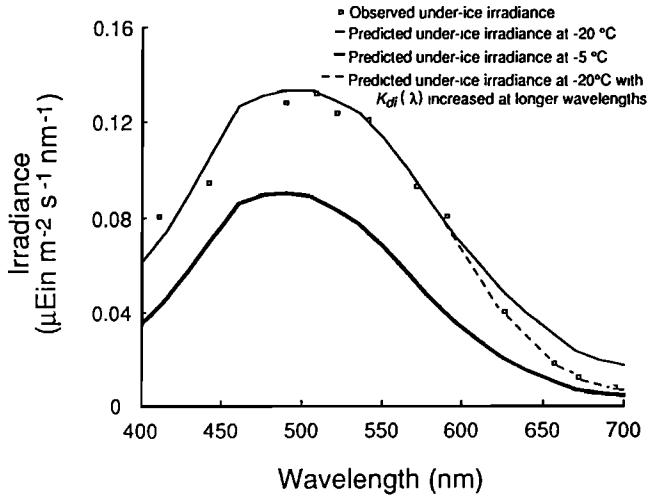

Fig. 10. Comparison of observed under-ice spectral irradiance in McMurdo Sound on September 27, 1984 (open squares), with model predictions. To test the effect of brine volume changes on predicted under-ice spectral irradiance, surface temperature was changed from -5°C to -20°C (both solid curves). A similar simulation verified that improved predictions could be obtained by increasing $K_{di}(\lambda)$ linearly 1-11% from 600 to 700 nm (dashed curve). Model input included measured congelation and platelet ice thickness (1.54 and 0.45 m, respectively), percent cloud cover (0), and chlorophyll *a* concentration (< 0.1 mg m^{-3}).

sheet. At -20°C, however, brine volume at the sea ice surface would be reduced to 26 ppt (the brine volume at the bottom remains unchanged due to its constant temperature of -1.8°C), with the ice sheet averaging only 43 ppt. Based upon the relationship shown in Figure 1, attenuation near the sea ice surface would be expected to be greater in the former case. It appears that the simulated reduction of $K_{di}(\lambda)$, due to lower brine volume and volume scattering, results in an enhancement of downwelling spectral irradiance at lower temperatures consistent with field observations.

The above examples indicate that the bio-optical model adequately describes radiative transfer in sea ice when particle concentrations are low. The remainder of this section will focus on the performance of the model under conditions of rapidly changing surface irradiance, surface temperature, sea ice thickness, and particle concentration.

Temporal Variation in Under-Ice PAR

Surface and under-ice PAR were measured in McMurdo Sound throughout the austral spring and early summer of 1984. Data for congelation and platelet ice thicknesses, chl *a* and phaeopigment concentrations, and profiles of ice temperatures were also collected (Table 2). This information was used as input for a series of runs designed to assess the model's accuracy on a diel (throughout the day) and seasonal basis when both the incident irradiance field and sea ice particulate concentrations were changing rapidly. The results for these runs, along with measured under-ice irradiance, are shown in Figures 11 through 13.

Figure 11 depicts a comparison of the predicted seasonal changes in the diel pattern of under-ice PAR with direct field observations. Predicted noon surface irradiance is shown for each run. Good agreement is obtained for both the diel patterns and the seasonal changes in under-ice irradiance. Most of the larger discrepancies are due to the assumption of a clear sky. For example, surface irradiance measurements (not presented) indicate, and field observations confirm, that variable cloud cover resulted in the model overestimating surface and under-ice PAR for the early part of the day on October 7. At noon, however, when skies had cleared, model predictions improved dramatically.

The model also accurately predicted a seasonal decrease in the intensity of under-ice PAR, despite the fact that surface PAR increased. On September 28, noon surface downwelling PAR was 470 μEin m^{-2} s^{-1} and under-ice PAR was 25 μEin m^{-2} s^{-1}, or 5% of the surface value. By December 5, however, noon surface PAR increased to 1335 μEin m^{-2} s^{-1} while under-ice PAR has decreased to 2 μEin m^{-2} s^{-1}, only 0.15% of surface PAR. This decrease in the percentage of transmitted irradiance resulted in part (21.7%) from increasing sea ice thickness (1.55 to 1.78 m), but is caused primarily by increasing particle concentrations (30 to 315 mg chl *a* m^{-2}) as a result of the spring algal bloom.

Diel Variation in Under-Ice Spectral Irradiance

A comparison of observed diel changes in under-ice spectral irradiance on December 5 with model predictions shown in Figure 12 illustrates the ability of the bio-optical model to account for changes in Sun angle and consequently, surface spectral irradiance when predicting under-ice irradiance. The magnitude and spectral form of predicted under-ice irradiance is nearly identical to field observations throughout the day (only values between midnight and noon are shown for clarity). In addition, absorption by high concentrations of photosynthetic pigment is apparent in both predicted and observed irradiance spectra as indicated by the presence of a 570-nm transmission peak and a slight transmission increase between 675 and 700 nm due to the secondary peak in chl *a* absorption at 680 nm.

Interestingly, Figure 12 indicates that while ice algae which are fixed vertically are exposed to changes in the amount of in-

TABLE 2. Input Parameters Used in Model Tests

Parameter	Sept. 27-28	Oct. 6-7	Oct. 26-27	Nov. 12-13	Nov. 4-25	Dec. 4-5
Snow depth, m*	0	0	0	0	0	0
Congelation ice depth, m*	1.55	1.66	1.78	1.80	1.80	1.78
Platelet ice depth, m*	0.50	0.53	0.50	0.50	0.50	0.48
Surface temperature, °C*	-20	-15	-9	-6	-3	-2
Cloud cover (0-10)	0	0	0	0	0	0
Chlorophyll *a* in congelation ice, mg m^{-2}*	5	15	40	50	60	65
Chlorophyll *a* in platelet ice, mg m^{-2}*	25	50	100	150	200	250
Detrital absorption (as percent of algal absorption)	0	0	5	10	15	20

Detrital absorption was estimated from phaeopigment concentrations given in Figure 6.
* Indicates field collected data.

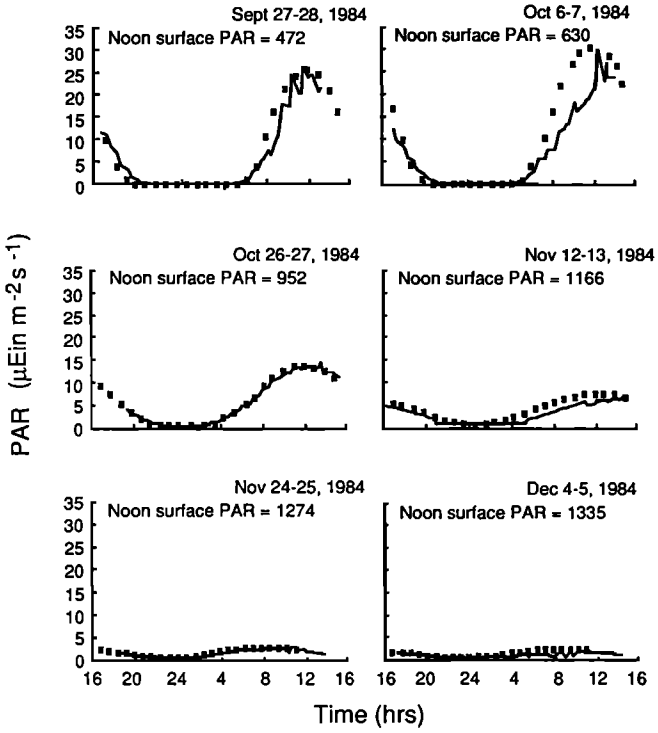

Fig. 11. Predicted (squares) versus observed (solid curves) seasonal changes in the pattern of diurnal under-ice PAR during development of the spring sea ice microalgal bloom of 1984 in McMurdo Sound, Antarctica. Noontime surface PAR is indicated on each graph. Table 2 shows the input for each simulation.

cident PAR, its spectral distribution remains relatively unchanged. This is unlike phytoplankton which mix through the water column and experience diel changes in both total irradiance and spectral distribution. Vertical stability may have important implications for the ability of sea ice algae to adapt their photosynthetic apparatus to efficiently utilize the available irradiance in this extreme light environment.

Seasonal Variation in Under-Ice Spectral Irradiance

Noon values for under-ice irradiance exhibited seasonal changes in spectral composition (Figure 13) in addition to the previously mentioned diel changes in spectral irradiance (Figure 12) and seasonal changes in PAR (Figure 11). Although predicted spectral irradiance may span more than an order of magnitude, only minor inconsistencies are apparent. These occur at wavelengths of 650-700 nm early in the season (September 28, October 7, and October 27), and in the 500-550 nm range later (November 13, November 25, and December 5).

The overestimates in spectral irradiance observed at wavelengths of 650-700 nm are most likely due to the previously mentioned underestimate of $K_{di}(\lambda)$ at longer wavelengths (see Figure 9). This can be shown by increasing $K_{di}(\lambda)$ linearly from 0 to 11% in the red wavelengths (0% increase at 600 nm to an 11% increase at 700 nm) which yields much better agreement (Figure 10). Because the values for $K_{di}(\lambda)$ used in the model were derived from radiative transfer theory, it appears that the diffuse attenuation for pure sea ice is greater than theory predicts at longer wavelengths within the visible (as shown above), or instrument sensitivity is inadequate in this range. *Grenfell* [1983] assumed the latter to be true when comparing his estimates of $K_{di}(\lambda)$ to observations made in the Arctic. However, Figure 13 (e. g. November 1984) reveals that acceptable precision was obtained under conditions of very low irradiance, indicating that the spectroradiometer used in this study was sufficiently sensitive.

Differences between predicted and observed under-ice spectral irradiance late in the season (November 13, November 25, and December 5) are more difficult to interpret. Due to the fact that agreement is good between 400 and 500 nm and from 575 to 700 nm, and model results for pure sea ice showed no deviation in the 500-550 nm range (Figure 9), it is unlikely that the observed differences are due to an overestimate of $K_{di}(z,\lambda)$ in that range. These dates occur late in the microalgal bloom when bulk spectral diffuse attenuation in sea ice is greatly influenced by the high particulate concentrations present (K_{di}=2.1 m^{-1} and K_{dp}=1.7 m^{-1} on December 5), indicating that the discrepancy may be due to variations in the optical characteristics of the microbial community related to photoadaptation. In support of this view, difference spectra calculated from absorption coefficients for sea ice algae collected from the upper and lower portions of the ice sheet indicate that by modifying pigment concentrations, ice algae are able to enhance absorption in the 450-550 nm range (Figure 14). These wavelengths coincide with the spectral region of poorest fit between observations and model predictions, suggesting that default specific absorption spectra for ice algae used in the model may differ from those of the community in situ in 1984. This is not surprising since specific absorption spectra can vary widely between species (Figure 4) and neither community- nor species-specific absorption spectra were determined during 1984 for the populations present at the time spectral irradiance measurements were made, necessitating the use of default spectra.

Model predictions of noon under-ice spectral irradiance on December 5 (conditions as shown in Table 2, except for detrital absorption which was 0%) show poor agreement with observed spectra in the 400-550 nm range, indicating that simulated values for K_d are too low in that region (Figure 15). There are at least two possible explanations for this. First, although attenuation by bacteria is ignored in the model, their absorption coefficient is similar spectrally to that of detritus [*Chamberlin*, 1989], and is thought to be important to radiative transfer in other systems [*Kiefer et al.*, 1990]. An unusually high concen-

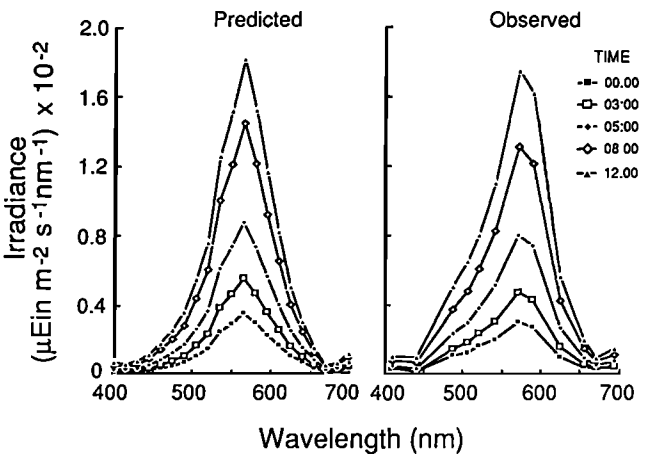

Fig. 12. Predicted versus observed diel changes in under-ice spectral irradiance on December 5, 1984. The time shown represents the time of day each measurement was taken and the time used as input for diel simulations. Table 2 (December 5) shows additional input for each simulation.

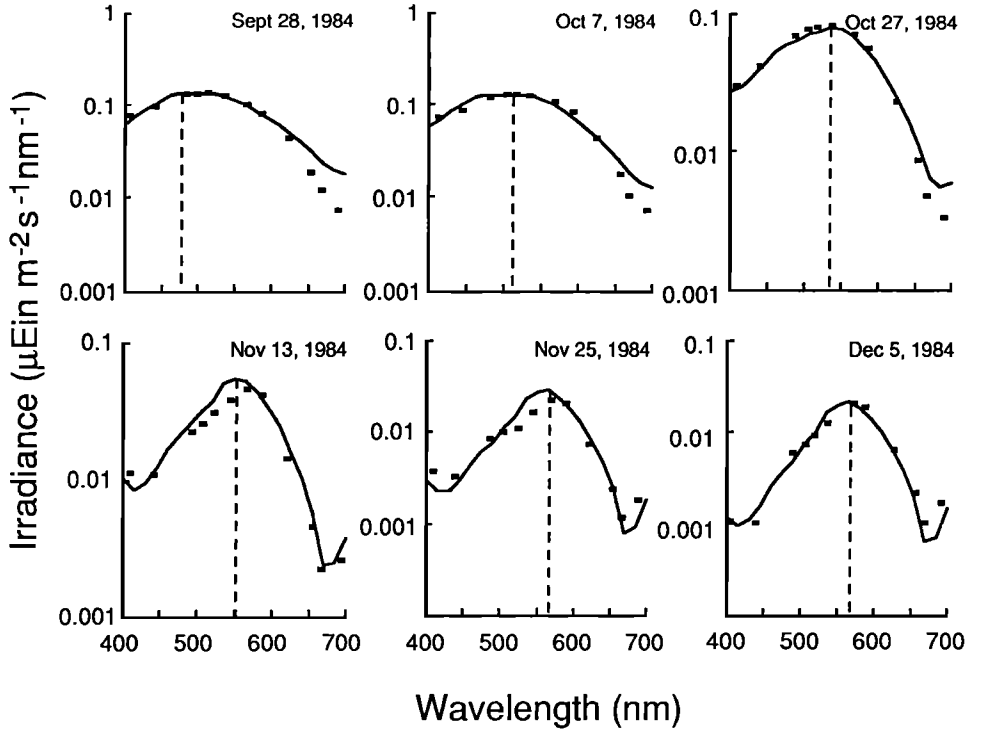

Fig. 13. Predicted (solid curves) versus observed (squares) under-ice spectral irradiance measured at local noon during development of the spring sea ice microalgal bloom of 1984 in McMurdo Sound, Antarctica (note log scale of irradiance). Table 2 shows additional input for each simulation.

tration of bacteria late in the season (December 5) might account for the observed differences in under-ice spectral irradiance. This is unlikely, however, because unlike the open ocean where bacterial biomass is generally equivalent to 10-40% of phytoplankton biomass [*Ducklow*, 1983], bacteria amount to less than 1% of algal biomass in land fast sea ice [*Kottmeier et al.*, 1987], even late in the season when bacteria reach peak abundance (3.3 x 10^{11} cells m^{-3}). In addition, the absorption coefficient for open ocean bacterioplankton at a concentration of 1 x 10^{12} cells m^{-3} is approximately 3.8 x 10^{-3} m^{-1} at 400-415 nm [*Stramski and Kiefer*, 1990]. Assuming sea ice bacteria exhibit similar optical properties, they would have no more than a minor impact on under-ice irradiance at typical concentrations.

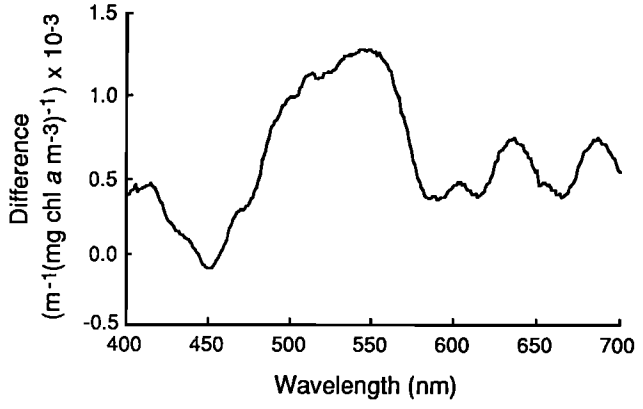

Fig. 14. Difference spectra of spectral specific absorption coefficients obtained from platelet and congelation ice microalgal communities (platelet - congelation) collected from McMurdo Sound, Antarctica, in November 1988.

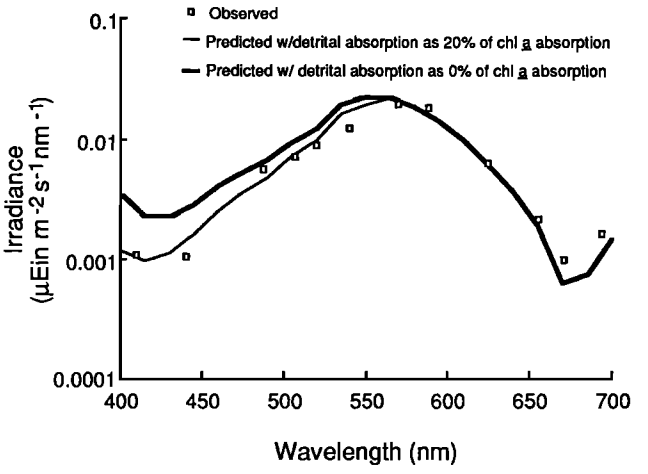

Fig. 15. Comparison of observed noontime under-ice spectral irradiance measured on December 5, 1984 (open squares), with model predictions assuming detrital absorption was equivalent to 0% (thick solid curve) and 20% (thin solid line) of total microalgal absorption. Table 2 shows additional input for each simulation.

An alternative explanation is that on December 5, detrital absorption was higher than the value of 0% used in early season model runs. This idea is supported by fluorometric pigment data obtained from sea ice particulate matter which indicates that as the spring bloom in McMurdo Sound progresses, the percent contribution by phaeopigments (an indicator of detritus) to total pigment concentration (chl *a*+phaeopigments) increases (Figure 6). Because phaeopigments are degradation products of chl *a* caused by grazing, such changes would be consistent with enhanced grazing pressure due to improved access of cryopelagic grazers to the microalgae as ice begins to

deteriorate. When the simulation for that day is run assuming 20% detrital absorption, agreement improves dramatically (Figure 15).

Finally, several simulations were carried out to see how predicted under-ice spectral irradiance changes as a function of species composition and microalgal photoadaptive state. When assuming a high algal biomass, the under-ice irradiance spectrum produced using values of $a^*(\lambda)$ for *Nitzschia stellata* in the 450-550 nm range from that obtained for *Nitzschia stellata* collected from the platelet ice (low light) (Figure 16). This phenomenon is even more pronounced when we compare these spectra to that obtained using $a^*(\lambda)$ estimated for the diatom *Auricula compacta* (Figure 4). These results indicate that taxonomic differences within the algal community may be observable in spectral radiometric measurements when individual species are in sufficiently high concentrations, and radiometers provide data with sufficient spectral resolution.

Results also illustrate how differences in sea ice microalgal concentration, species composition, and photoadaptive state can affect under-ice spectral irradiance, which may in turn significantly alter the rate of photosynthesis within the water column.

USES OF THE BIO-OPTICAL MODEL

In Situ Versus Laboratory Estimates of Primary Productivity

It is common practice to use estimates of ^{14}C-radioactive carbon fixation by algae in the laboratory to infer rates of primary production for field populations [*Lewis and Smith*, 1983]. Accurate estimates of primary production can only be made by this method, however, if the spectral output of the incubator light source is the same as that found in situ. This is because all wavelengths within the visible are not absorbed with equal efficiency, and consequently, observed rates of photosynthesis are a function of the spectral distribution of incident irradiance.

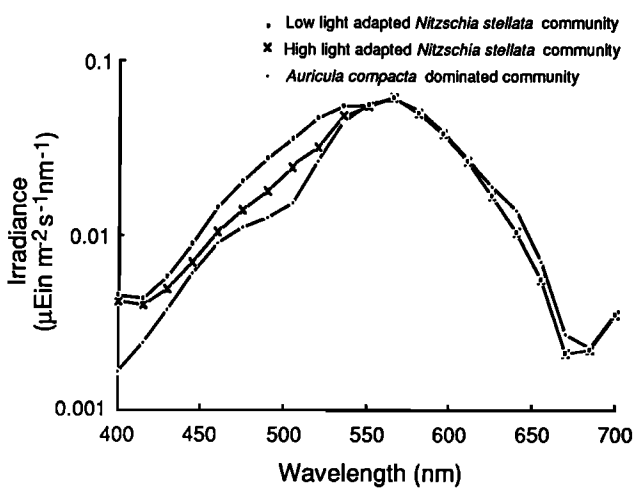

Fig. 16. Predicted under-ice spectral irradiance as a function of photoadaptive state and species composition of the microbial community. The specific absorption spectra obtained from high and low light adapted *Nitzschia stellata* represent the extremes seen for this species (Figure 4) and result in distinct differences in predicted under-ice spectral irradiance. Using the high specific absorption coefficient obtained from *Auricula compacta* (Figure 4) results in even lower predicted under-ice spectral irradiance. Table 2 (December 5) shows additional input for each simulation.

Because the spectral irradiance where sea ice microalgae reside is difficult to measure, the bio-optical model makes it possible to obtain reasonable estimates. Laboratory-based estimates of primary production and photosynthetic parameters such as α (photosynthetic efficiency), β (photoinhibition), and I_k (photoadaptation) can be corrected to reflect better the field conditions and photophysiological characteristics of the algae.

The correction consists of converting measurements of PAR made both in the field and in the experimental setup to PUR. According to *Morel* [1978],

$$\mathrm{PUR}(z) = \int_{400}^{700} a(z,\lambda)\, E(z,\lambda)\, d\lambda \tag{10}$$

where $a(z,\lambda)$ is the spectral absorption coefficient for the community normalized to its maximum value (at 440 nm) and $E(z,\lambda)$ is the ambient spectral irradiance (predicted or observed). PUR represents the proportion of downwelling irradiance absorbed by algal cells and is dependent upon the absorption properties of the algae and the spectral distribution of downwelling irradiance. Photosynthetic rates related experimentally to PUR may then be combined with estimates of PUR (predicted or measured) in situ to obtain more realistic estimates of primary productivity.

Estimating Algal Stocks

The bio-optical model can be used in conjunction with surface and under-ice spectral irradiance measurements from remotely operated or manned submersibles to obtain 2-dimensional maps of chl *a* concentrations in sea ice. From equation (2) the bulk diffuse attenuation coefficient for sea ice can be written as

$$K_d(\lambda) = K_{di}(\lambda) + K_{dp}(\lambda) \tag{11}$$

or by rearrangement,

$$K_{dp}(\lambda) = K_d(\lambda) - K_{di}(\lambda) \tag{12}$$

Variable subscripts are as defined for equation (2). The value for $K_d(\lambda)$ can be determined by measuring surface and under-ice irradiance, and $K_{di}(\lambda)$ can be estimated with the bio-optical model using known values for surface temperature and sea ice thickness. Once $K_{dp}(\lambda)$ has been determined, equations (3), (4) and (6) through (9) can be combined to yield the following relationship between the mean chl *a* concentration in the ice sheet and $K_{dp}(\lambda)$:

$$C = \frac{K_{dp}(\lambda)\,\bar{\mu}}{abs} \tag{13a}$$

where

$$abs = a^*(\lambda) + \frac{\delta \int_{400}^{700} a^*(\lambda)\, d\lambda}{\int_{400}^{700} e^{-0.008(\lambda-400)}\, d\lambda}\, e^{-0.008(\lambda-400)} \tag{13b}$$

C is the mean chl *a* concentration (mg m^{-3}) for the ice sheet (which can be converted to units of mg m^{-2} by multiplying by the sea ice thickness) and $\int e^{-0.008(\lambda-400)}\, d\lambda = 113.8$ when inte-

grated from 400 to 700 nm. Values for $K_{dp}(\lambda)$, $e^{-0.008(\lambda-400)}$, and $a^*(\lambda)$ need only be specified at a single wavelength to estimate chl *a* concentration using equation (13). However, the value for $\int a^*(\lambda)\, d\lambda$ depends upon the particular specific absorption coefficient spectrum used.

Obviously, the accuracy of this approach depends upon the proper estimation of the detrital absorption term, δ. Fortunately, during much of the algal bloom, δ is probably <10%. Only at the latest stages of bloom development are larger values for δ likely to be encountered. However, even this would introduce substantial errors into the estimation of chl *a* concentration only if phaeopigment concentrations in the field cannot be estimated with reasonable certainty.

Ecosystem Models

Finally, the bio-optical model can be coupled to other models of sea ice dynamics to produce an ecosystem model which couples microalgal growth and production to conditions of the physicochemical environment. Models simulating many of the physical processes known to occur in sea ice, including sea ice growth [*Maykut,* 1986], desalination [*Cox and Weeks,* 1988], and nutrient flux [*Wakatsuchi and Ono,* 1983] can be combined with the present bio-optical model to describe the environmental factors thought to be most influential in controlling microalgal growth: temperature, spectral irradiance, nutrient concentration, and salinity. Used in conjunction with knowledge of the physiological and growth characteristics of sea ice microalgae, this ecosystem model may then be used to estimate seasonal changes in primary production as well as to test our understanding of the relative importance of the various physicochemical influences on primary production. Such a model currently is under development [*Arrigo et al.*, 1990].

Acknowledgments. We thank S. T. Kottmeier for collection of spectral irradiance data during 1984, R. Iturriaga for single cell absorption data, and D. Robinson and R. Reynolds for their assistance in data collection in 1988 and 1989 and helpful discussions concerning particulate absorption. We extend special thanks to D. Stramski and T. Grenfell for numerous helpful comments and suggestions during the development of both the model and manuscript. This work was supported by NSF grants DPP-817237 and DPP-8717692 from The Division of Polar Programs; and by ONR grant N00014-88-0187.

REFERENCES

Arrigo, K. R., C. W. Sullivan, and J. N. Kremer, A model of a sea ice ecosystem, McMurdo Sound, Antarctica, paper presented at 22nd International Liege Colloquium on Ocean Hydrodynamics, Liege, Belgium, May 7-11, 1990.

Bidigare, R. R., R. C. Smith, K. S. Baker, and J. Marra, Oceanic primary production estimates from measurements of spectral irradiance and pigment concentrations, *Global Biogeochemical Cycles, 1*, 171-186, 1987.

Brine, D. T., and M. Iqbal, Diffuse and global solar spectral irradiance under cloudless skies, *Sol. Energy, 30*, 447-453, 1983.

Bunt, J. S., and C. C. Lee, Seasonal primary production in Antarctic sea ice at McMurdo Sound in 1967, *J. Mar. Res, 28*, 304-320, 1970.

Chamberlin, W. S., Light absorption, natural fluorescence, and photosynthesis in the open ocean, Ph.D. thesis, Univ. of South. Calif., Los Angeles, 1989.

Cox, G. F. N., and W. F. Weeks, Brine drainage and initial salt entrapment in sodium chloride ice, *Res. Rep. 345*, U.S. Army Cold Reg. Res. Eng. Lab., Hanover, N. H., 1975.

Cox, G. F. N., and W. F. Weeks, Equations for determining the gas and brine volumes of sea-ice samples, *J. Glaciol., 29*, 306-316, 1983.

Cox, G. F. N., and W. F. Weeks, Changes in the salinity and porosity of sea-ice samples during shipping and storage, *J. Glaciol., 32*, 371-375, 1986.

Cox, G. F. N., and W. F. Weeks, Profile properties of undeformed first-year sea ice, *Res. Rep. 88-13*, U.S. Army Cold Reg. Res. Eng. Lab., Hanover, N. H, 1988.

Ducklow, H. W., Production and fate of bacteria in the ocean, *Bioscience, 33*, 494-501, 1983.

Grenfell, T. C., and G. A. Maykut, The optical properties of ice and snow in the Arctic basin, *J.Glaciol., 18*, 445-463, 1977.

Grenfell, T. C., A theoretical model of the optical properties of sea ice in the visible and near infrared, *J. Geophys. Res., 88*, 9723-9735, 1983.

Grenfell, T. C., and D. K. Perovich, Radiation absorption coefficients of polycrystalline ice from 400-1400 nm, *J. Geophys. Res., 86*, 7447-7450, 1981.

Grenfell, T. C., and D. K. Perovich, Optical properties of ice and snow in the polar oceans, I, Observations, *Proc. SPIE Int. Soc. Opt. Eng., 637*, 242-251, 1986.

Grossi, S. M., S. T. Kottmeier, R. L. Moe, G. T. Taylor, and C. W. Sullivan, Sea ice microbial communities, VI, Growth and primary production in bottom ice under graded snow cover, *Mar. Ecol. Prog. Ser., 35*, 153-164, 1987.

Iturriaga, R., and C. W. Sullivan, Spectral light absorption characteristics of individual sea ice microalgae from McMurdo Sound, Antarctica, *Antarct. J. U.S., 24*, 188-190, 1989.

Iturriaga, R., B. G. Mitchell, and D. A. Kiefer, Microphotometric analysis of individual particle absorption spectra, *Limnol. Oceanogr., 27*, 492-499, 1988.

Kiefer, D. A., and J. B. SooHoo, Spectral absorption by marine particles of coastal waters of Baja California, *Limnol. Oceanogr., 27*, 492-499, 1982.

Kiefer, D. A., J. H. Morrow, D. Stramski, and W. S. Chamberlin, An electron transport hypothesis for seasonal changes in the spectral absorption coefficient of particles in the Western Sargasso Sea (abstract), *Eos Trans. AGU, 71*, 97, 1990.

Kirk, J. T. O., *Light and Photosynthesis in Aquatic Ecosystems*, pp. 24-41, Cambridge University Press, New York, 1983.

Kottmeier, S. T., S. M. Grossi, and C. W. Sullivan, Sea ice microbial communities, VIII, Bacterial production in annual sea ice of McMurdo Sound, Antarctica, *Mar. Ecol. Prog. Ser., 35*, 175-186, 1987.

Lewis, E. L., and W. F. Weeks, Sea ice: Some polar contrasts, *Symposium on Antarctic Ice and Water Masses, Scientific Committee on Antarctic Research*, Tokyo, 1970.

Lewis, M. R., and J. C. Smith, A small volume, short incubation time method for measurement of photosynthesis as a function of incident irradiance, *Mar. Ecol. Prog. Ser., 13*, 99-102, 1983.

Maykut, G. A., and T. C. Grenfell, The spectral distribution of light beneath first-year sea ice in the Arctic Ocean, *Limnol. Oceanogr., 20*, 554-563, 1975.

Maykut, G. A., The surface heat and mass balance, in *The Geophysics of Sea Ice*, edited by N. Untersteiner, pp. 395-463, Plenum, New York, 1986.

Morel, A., Available, usable and stored radiant energy in relation to marine photosynthesis, *Deep Sea Res., 25*, 673-688, 1978.

Morel, A, and A. Bricaud, Theoretical results concerning light absorption in a discrete medium, and application to specific absorption of phytoplankton, *Deep Sea Res., 28*, 1375-1393, 1981.

Palmisano, A. C., and C. W. Sullivan, Sea ice microbial communities (SIMCO), I, Distribution, abundance, and primary production of ice microalgae in McMurdo Sound, Antarctica in 1980, *Polar Biol., 2*, 171-177, 1983.

Palmisano, A. C., J. B. SooHoo, R. L. Moe, and C. W. Sullivan, Sea ice microbial communities, VII, Changes in under-ice spectral irradiance during the development of Antarctic sea ice microalgal communities, *Mar. Ecol. Prog. Ser., 35*, 165-173, 1987.

Perovich, D. K., The optical properties of young sea ice, M.S. thesis, 151 pp.,Univ. of Wash., Seattle, 1979.

Perovich, D. K., A two-stream multilayer, spectral radiative transfer model for sea ice. *Res. Rep. 89-15*, U.S. Army Cold Reg. Res. Eng. Lab., Hanover, N. H., 1989.

Perovich, D. K., and T. C. Grenfell, A theoretical model of radiative transfer in young sea ice, *J. Glaciol., 28*, 341-356, 1982.

Perovich, D. K., G. A. Maykut, and T. C. Grenfell, Optical properties of ice and snow in the polar oceans, I, Observations, *Proc. SPIE Int. Soc. Opt. Eng., 637*, 232-244, 1986.

Preisendorfer, R. W., *Hydrologic Optics, vol. VI*, U.S. Department of Commerce, Honolulu, 1976.

Reifsnyder, W. E., and H. W. Lull, Radiant energy in relation to forests, *Tech. Bull. 1344*, U.S. Dep. of Agric., Washington, D. C., 1965.

Sathyendranath, S., L. Lazarra, and L. Prieur, Variations in the spectral values of specific absorption of phytoplankton, *Limnol. Oceanogr.*, *32*, 403-415, 1987.

Sathyendranath, S., T. Platt, C. M. Caverhill, R. E. Warnock, and M. R. Lewis, Remote sensing of oceanic primary production: Computations using a spectral model, *Deep Sea Res.*, *36*, 431-453, 1989.

Smith, R. C., and K. S. Baker, The bio-optical state of ocean waters and remote sensing, *Limnol. Oceanogr.*, *23*, 247-259, 1978.

SooHoo, J. B., A. C. Palmisano, S. T. Kottmeier, M. P. Lizotte, S. L. SooHoo, and C. W. Sullivan, Spectral light absorption and quantum yield of photosynthesis in sea ice microalgae and a bloom of *Phaeocystis pouchetii* from McMurdo Sound, Antarctica, *Mar. Ecol. Prog. Ser.*, *39*, 175-189, 1987.

Spencer, J. W., Fourier series representation of the position of the sun, *Search*, *2*, 172, 1971.

Stephenson, P. J., Some considerations of snow metamorphism in the Antarctic ice sheet in the light of crystal studies, in *Physics of Snow and Ice, Proc. International Conference on Low Temperature Sciences, 14-19 August 1966*, edited by H. Oura, pp. 725-740, Bunyeido Printing Company, Sapporo, Japan, 1967.

Stramski, D., and D. A. Kiefer, Optical properties of marine bacteria, *Proc. SPIE Int. Soc. Opt. Eng.*, *1302*, 250-268, 1990.

Sullivan, C. W., and A. C. Palmisano, Sea ice microbial communities: Distribution, abundance, and diversity of ice bacteria in McMurdo Sound, Antarctica, in 1980, *Appl. Env. Microbiol.*, *47*, 788-795, 1984.

Sullivan, C. W., A. C. Palmisano, S. T. Kottmeier, S. McGrath Grossi, and R. Moe, The influence of light on growth and development of the sea-ice microbial community of McMurdo Sound, in *Antarctic nutrient cycles and food webs*, edited by W. R. Siegfried et al., 78-83, Springer-Verlag, New York, 1985.

Thorndike, A. S., D. A. Rothrock, G. A. Maykut, and R. Colony, The thickness distribution of sea ice, *J. Geophys. Res.*, *80*, 4501-4513, 1975.

Wadhams, P., The seasonal ice zone, in *The Geophysics of Sea Ice* edited by N. Untersteiner, pp. 825-991, Plenum, New York, N.Y., 1986.

Wakatsuchi, M., and N. Ono, Measurements of salinity and volume of brine excluded from growing sea ice, *J. Geophys. Res.*, *88*, 2943-2951, 1983.

K. R. Arrigo and J. N. Kremer, Department of Biological Sciences, University of Southern California, Los Angeles, CA 90089-0371.

C. W. Sullivan, Graduate Program in Ocean Sciences, Hancock Institute of Marine Studies, University of Southern California, Los Angeles, CA 90089-0373.

(Received July 26, 1990;
revised January 4, 1991;
accepted January 22, 1991.)